Science Progress (2015), 98(1), 34–62
Doi:10.3184/003685015X14234978376369

Advances in antihydrogen physics

MIKE CHARLTON and DIRK PETER VAN DER WERF

Mike Charlton (left; E-mail: m.charlton@swansea.ac.uk) and Dirk Peter van der Werf (right; E-mail: d.p.van.der.werf@swansea.ac.uk) are both Professors of Physics at Swansea University.

They are part of a Swansea team involved in the ALPHA antihydrogen collabortion. This project previously scored a pioneering breakthrough by trapping atoms of antihydrogen for more than 16 minutes – a significant improvement on past efforts. The Swansea group were joint winners of the American Physical Society's 2011 John Dawson Award for their work on the breakthrough.

ABSTRACT

The creation of cold antihydrogen atoms by the controlled combination of positrons and antiprotons has opened up a new window on fundamental physics. More recently, techniques have been developed that allow some antihydrogen atoms to be created at low enough kinetic energies that they can be held inside magnetic minimum neutral atom traps. With confinement times of many minutes possible, it has become feasible to perform experiments to probe the properties of the antiatom for the first time. We review the experimental progress in this area, outline some of the motivation for studying basic aspects of antimatter physics and provide an outlook of where we might expect this field to go in the coming years.

Keywords: *antimatter, antihydrogen, positron, antiproton, positronium*

1. Introduction

Antimatter has long held a grip on the fascination of both scientists and the general public, though usually for very different reasons. Dirac's famous 1931 prediction of the existence of both the positron and the antiproton[1] (though he did confess to know nothing of the nature of the proton) holds a special place in physics. That the concept of antiparticles could arise from the unification of two such basic theories as quantum mechanics and special relativity places antimatter at the heart of fundamental science. A much more complete understanding of its role was forthcoming with the development of quantum field theory and an appreciation of the importance of symmetries in physics. It is now known that, in local quantum field theories that obey the usual rules of spin statistics and are Lorentz invariant, the properties of antimatter are constrained to be absolutely equal to, or equal in magnitude to, those of their matter counterparts. This is formalised in the famous CPT theorem, in which the combined operation of charge conjugation (C), parity reversal (P) and time reversal (T) transforms a particle into an antiparticle (and *vice versa*) with the same momentum. This theorem also implies that the energy levels of systems linked by the CPT transformation (for example, hydrogen and antihydrogen) are identical.

Nonetheless, there is great interest in performing measurements of the spectral properties of antihydrogen for comparison with those of hydrogen. Some of the latter, such as the frequencies of the 1S – 2S two-photon transition[2] and the ground state hyperfine splitting[3] are known to incredible accuracy, such that precise and direct tests of CPT may be forthcoming if antihydrogen can be studied in a similar depth. Why tests of CPT are topical is due to one of the major conundrums of modern physics; namely, the apparent fate of antimatter in the early Universe. It seems that we live in a matter-dominated Universe (though searches for signs of cosmic antimatter continue, notably recently with the observational campaigns of the PAMELA[4,5] and AMS-02[6,7] collaborations) in which all of the antimatter disappeared as the Universe cooled after the Big Bang. This implies that two distinct events occurred with the disappearance of the antiquarks, and then the positrons. Thus, once the Universe had cooled sufficiently that atomic systems (principally hydrogen) could be formed, there were no antiparticles remaining to create antihydrogen. It is widely thought that this implies that there are deep matter–antimatter asymmetries in the laws of physics that we have not yet uncovered, and this in part motivates the antihydrogen studies.

From a theoretical perspective, the received wisdom, aka The Standard Model, is that CPT is conserved, since the CPT theorem[8,9] is a cornerstone of modern quantum field theories. Violations of the constituent symmetries and pairwise combinations (most famously CP) are known and are incorporated in the Standard Model. It is notable, though, that many experimental searches are under way for further examples of CP (or T) violation in an effort to understand the dearth of antimatter; currently the size of the known violations is many orders of magnitude too small to explain the baryon density of the Universe. Phenomenological extensions to the Standard Model (so-called SME theories) have been developed, in particular by Kostelecký and co-workers (see for example ref. 10 for a summary of a selection of that work). In SME, additional coupling terms are added to a Standard Model Lagrangian and their effects on various parameters (such as the spectroscopic properties of antihydrogen) can be evaluated and, where measurements are available, may be used to set limits on SME effects, such as CPT and Lorentz symmetry violations.

As will be described in this article, several experiments are aiming to make measurements of the gravitational acceleration of antihydrogen. (Other antiparticle-containing systems, such as positronium and muonium are also the subject of planned gravity measurements, but such efforts are beyond the scope of this contribution.) Despite many years of (mainly) theoretical speculation (see, for example, refs 10 and 11) there have been no direct tests of antimatter gravity. Arguments concerning limits set by considering the virtual antimatter content of ordinary matter subject to Eötvos-type torsion balance experiments[13] are not uniformly accepted. Again, the conventional expectation is that based upon General Relativity, the Weak Equivalence Principle (WEP) should hold for antimatter as it does for matter. However, it is widely appreciated that, at a fundamental level not yet understood, quantum mechanics and general relativity are incompatible. Thus, WEP tests for antimatter have recently arrived onto the experimental agenda, and we can look forward to progress in this area in the coming decade.

The remainder of this article is organised as follows. In Section 2 we present, hopefully in an accessible fashion, some of the instrumentation and techniques that have been developed in order to facilitate experiments with antihydrogen. Sections 3 and 4 contain summaries of the results from the antihydrogen production, trapping and

investigatory experiments to date. We end with some conclusions and an outlook in Section 5. Our aim in this article is not to be comprehensive, nor to go into excessive detail in any aspect of the field, but rather to give the reader a background in the physics of an exciting new sub-branch of antimatter science which sits on the boundaries of particle, nuclear, atomic and plasma physics.

2. Experimental background

2.1 Preliminaries

For the first decade or so of the operation of the Antiproton Decelerator (AD)[14,15] facility at CERN, there were three main experiments involving antihydrogen, $\overline{\mathrm{H}}$: ALPHA (and its forerunner, ATHENA) and ATRAP, which were both antihydrogen-driven in their outlook, and ASACUSA, with a wide-ranging programme, also involving the antiprotonic helium atom (see, for example, ref. 16). These have been joined recently by AEgIS[17] and GBAR[18] which are both antimatter gravity efforts, and aspects of their progress are described herein.

The methodologies which are common to all of the efforts to date include positron (e^+) and antiproton ($\bar{p}$) capture, cooling and manipulation, their combination to form antihydrogen and the subsequent registration that an antiatom has formed. All experiments rely, of course, on the AD facility, part of the PS-complex of "accelerators" at CERN. The AD takes pulses of antiprotons with a momentum around 3.5 GeV/c created in collisions of 26 GeV/c protons with a fixed target. They are decelerated and cooled in a three-stage procedure lasting around 100 s to reach a beam momentum of 105 MeV/c, equivalent to a kinetic energy of 5.3 MeV. Thereafter they are ejected to the experiments in pulses of less than 300 ns duration, where, as described below, they are subject to further procedures to prepare them for antihydrogen formation.

The need for low energy, or cold, antiparticles for antihydrogen experimentation stems from the processes which are thought to underlie formation. The two main mechanisms are radiative combination, involving emission of a photon ($h\nu$), as:

$$\bar{p} + e^+ \rightarrow \overline{\mathrm{H}} + h\nu \tag{1}$$

and three-body combination given by

$$\bar{p} + e^+ + e^+ \rightarrow \overline{\mathrm{H}} + e^+. \tag{2}$$

The details of these reactions have been summarised elsewhere[10], suffice to say that, in equilibrium, they have very different dependencies on the temperature, T_e, of the positron cloud or plasma, produce very different antihydrogen states and depend upon the positron density n_e to the first [reaction (1)] and second [reaction (2)] powers. In particular, reaction (2), which is essentially a quasi-elastic collision of two positrons in the vicinity of an antiproton, produces antihydrogen in very weakly bound states that are susceptible to influence by the ambient electric and magnetic fields (for example, see refs 19 and 20) and has an equilibrium rate which varies as $T_e^{-4.5}$. Though there has been no direct observations of either of these reactions, evidence for three-body combination *via* the field ionisation of the weakly bound states produced has been forthcoming from ATHENA[21] and ALPHA[22], but particularly ATRAP, who developed field ionisation as a detection technique[23], and used it to obtain some information on the binding energies of the nascent antiatoms[24].

The two antimatter gravity experiments, AEgIS and GBAR, both intend to use positronium (Ps) as a means to antihydrogen *via* the charge exchange reaction,

$$\bar{p} + \mathrm{Ps} \rightarrow \overline{\mathrm{H}} + e^- \qquad (3)$$

where the Ps may be in an excited state. The use of this route was suggested some time ago[25–27]. One benefit of this reaction is that the cross-section extends over several (and perhaps several 10s of, dependent upon the Ps principal quantum number, n_{Ps}) keV of $\bar{p}$ kinetic energy. Thus a beam of monoenergetic $\overline{\mathrm{H}}$ can be created. This will be exploited by GBAR who wish to create the antihydrogen positive ion $\overline{\mathrm{H}}^+$ *via* another charge exchange reaction involving Ps, *viz* $\overline{\mathrm{H}} + \mathrm{Ps} \rightarrow \overline{\mathrm{H}}^+ + e^-$ [18]. Further benefits include major increases in reaction cross-section, which scales in the classical limit as n_{Ps}^4 [26] if Rydberg Ps can be produced, as was demonstrated recently[28]. Another possible bonus of using excited state Ps is that the reaction can occur with essentially stationary $\bar{p}$s and with the $\overline{\mathrm{H}}$ formed preferentially in states with binding energies very close to the parent Ps, the added recoil to the antihydrogen can be small[27,29]. This will be exploited by AEgIS who need a collimated, very cold, $\overline{\mathrm{H}}$ beam for their deflectometry experiments[17,30]; see Section 3.

Before describing techniques, it is perhaps worth dwelling here on two key pieces of apparatus for antihydrogen production and trapping, namely traps, both for the charged antiparticles and for the antiatoms. Both are shown in Figure 1 which provides a schematic illustration of the ALPHA apparatus. The charged particle traps employed are usually Penning-type devices, which have found a multitude of applications throughout physics and chemistry (see for example refs 31 and 32). These instruments employ a strong (typically of order Tesla), uniform magnetic field which is arranged along the axis of symmetry of a set of electrodes. The magnetic field ensures radial confinement of the charged particles, whilst appropriate voltages applied to the electrodes ensure axial confinement. In antihydrogen studies the electrodes are cylinders arranged in a stack

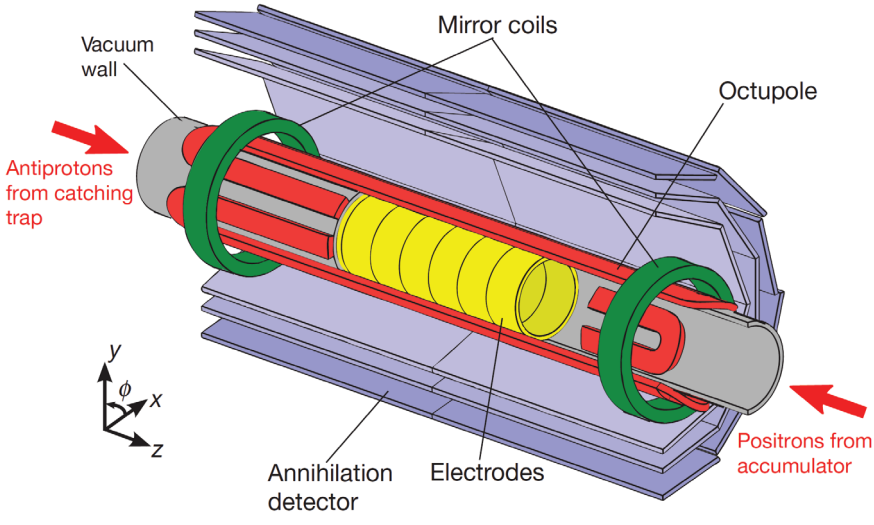

Figure 1 *Schematic illustration of the ALPHA apparatus showing the coil arrangement used to form the neutral atom trap and some of the electrodes used to provide axial confinement for the* $\bar{p}$s *and* e^+s. *An additional uniform magnetic field along the z-axis is provided by an external solenoid (not shown).*

along the magnetic field axis, and typically can be biased in a manner to ensure that several separate traps can be formed simultaneously for the collection and manipulation of the antiparticle clouds/plasmas. Examples can be found in the comprehensive descriptions available of the ATHENA and ALPHA apparatus[33,34].

In an ideal Penning trap, the single particle motion is well known, as described in Brown and Gabrielse's comprehensive review[35]. In a uniform magnetic field, say in the z-direction $\mathbf{B}=B\hat{\mathbf{z}}$, a charged particle of mass m and charge q will exhibit cyclotron motion around the field lines with an angular frequency $\omega_c=qB/m$. With the Penning-trap electric fields added the particles undergo axial oscillation with frequency $\omega_z=\sqrt{2qV/md^2}$, which is dependent upon the particular electrode geometry and the applied voltages *via* the parameters d and V respectively. The Penning configuration also produces $\mathbf{E}\times\mathbf{B}$ fields which modify ω_c into ω_+, and cause the particle to exhibit magnetron motion with a frequency ω_-. These two frequencies are related by $\omega_\pm=\frac{1}{2}\left(\omega_c\pm\sqrt{\omega_c^2-2\omega_z^2}\right)$, and in a typical arrangement for antihydrogen, $\omega_+\gg\omega_z\gg\omega_-$ for both $\bar{p}$ and e^+. Even when the trap potentials are non-ideal (and have so-called anharmonic components) these three motions can still be identified and in some instances their frequencies and/or amplitudes measured and modified if appropriate.

The devices used to hold antihydrogen by ALPHA and ATRAP are based upon magnetic minimum neutral atom traps, usually termed Ioffe–Pritchard traps[36,37]. Here a three-dimensional magnetic field minimum is used to hold onto atoms with the appropriate magnetic moment and low kinetic energy. Given that the shift of an energy level, U, of ground state antihydrogen in a magnetic field, $\mathbf{B}$ is given by $U=-\boldsymbol{\mu}_{\bar{\mathrm{H}}}\cdot\mathbf{B}$, with $\boldsymbol{\mu}_{\bar{\mathrm{H}}}=\boldsymbol{\mu}_{\mathrm{B}}$ the Bohr magneton, a field gradient can produce a restoring force, $\mathbf{F}_{\mathrm{B}}$ as

$$\mathbf{F}_{\mathrm{B}}=-\nabla(\boldsymbol{\mu}_{\bar{\mathrm{H}}}\cdot\mathbf{B}). \tag{4}$$

The field minimum is formed by the pair of mirror coils and, in ALPHA's case (Figure 1), an octupolar coil arrangement. The mirror coil fields vary along the axis as $B(z)=B(0)-\beta z^2$, where $z=0$ is located directly underneath each coil and β is a constant. The radial field of a multipolar coil of order s (*e.g.*, $s=2$ corresponds to a quadrupole, with $s=4$ an octupole) varies with radius r as $B_s(r)=K_s r^{s-1}$, with K_s a constant. The quadrupole is the configuration usually adopted in cold atom physics, and has been used by ATRAP (see ref. 38). ALPHA chose an octupolar configuration since the radial field, which has been shown to severely impair the long-term charged particle cloud or plasma confinement properties of Penning-type traps[39], is smaller close to $r=0$. Further discussion can be found elsewhere[34].

2.2 Antiparticle capture, cooling and manipulation

As described briefly in Section 2.1, the $\bar{p}$s are provided to experiments in bursts at a kinetic energy of 5.3 MeV. Most experiments then use a foil degrading technique[40] to slow a fraction (of order 0.1%) of them down so that they can be dynamically captured in a Penning trap. (The exception is ASACUSA, which pre-decelerates the $\bar{p}$s to 100 keV using an RFQ decelerator[41].) Typical Penning trap field strengths are several Tesla, as the capture efficiency is depressed at low fields[42].

The capture procedure is shown schematically in Figure 2. This illustrates how $\bar{p}$s entering the apparatus from the AD are slowed on traversing the thin degrader foil placed at the entrance to a Penning trap. Those with kinetic energies lower than about

5 keV are then dynamically captured using a voltage pulse applied to the foil, once the pulse of antiparticles has entered the trap. Prior to the arrival of the $\bar{p}$s a cloud of electrons (with a density typically in the range of 10^{14} m^{-3} and more numerous than the trapped antiproton yield by a factor of roughly 10^4) is loaded into a central region in the elongated trap. In the 3 T magnetic field used by ATHENA the cyclotron oscillation frequency of the electrons is of the order of 100 GHz, and as a result they lose kinetic energy rapidly *via* the emission of synchrotron radiation to reach a base temperature (close to, but not necessarily the same as, the trap ambient) within a fraction of a second[43]. The $\bar{p}$s pass to-and-fro through the electrons to which they couple *via* the Coulomb interaction, whereupon they lose their kinetic energy *via* collisions: energy

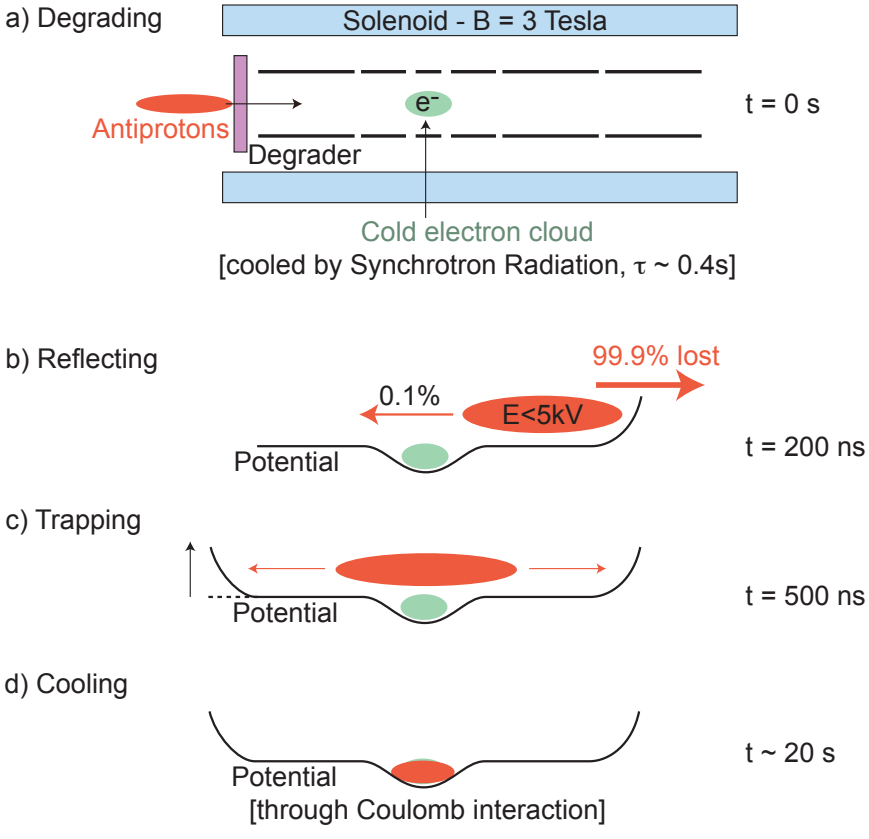

Figure 2 *Schematic illustration of antiproton trapping for antihydrogen formation. (This example is typical of the arrangement used by the ATHENA collaboration[33].) (a) Antiprotons enter in a burst from the AD, traversing a thin foil degrader before entering the Penning-type trap formed from the voltages applied to the cylindrical electrodes and the 3 T magnetic field provided by a solenoid. The trap is immersed in an ultra-high vacuum chamber, and is cooled to a temperature, in this case, of around 15 K. (b) Those* $\bar{p}$s *which emerge from the degrader with a kinetic energy less than around 5 keV are reflected by the voltage applied to an end cap electrode. (c) Around 500 ns after the* $\bar{p}$s *arrive a similar high voltage is applied to the degrader to capture the low energy antiparticles. (d) Prior to the* $\bar{p}$ *pulse a cloud of electrons has been loaded into a central trap, where they self-cool* via *the emission of synchrotron radiation. The trapped* $\bar{p}$s *interact with this cloud and lose kinetic energy in collisions. After 10–20 s the* $\bar{p}$s *reside in the central well with the electrons, and are cooled to their temperature.*

which is in turn radiated away by the electrons. After a few 10s of seconds or so, depending upon detailed experimental circumstances, the $\bar{p}$s reside in the small central well with the electron cloud. The latter can be ejected as required by applying rapid excitation pulses to them, such that only the more massive $\bar{p}$s remain confined in a volume of ~1 cm^3 in preparation for further experimentation leading to antihydrogen formation.

To create antihydrogen the antiprotons must be mixed with positrons, and how this is done will be described in Section 3. Positrons are the most readily available antiparticle, and may be produced in nuclear β-decay. Positrons have found numerous applications, particularly in materials science and medicine. In the latter, positron emission tomography (PET), is a well-established and widely available clinical diagnostic technique for functional imaging of the body (see, for example ref. 44). However, over 40 years ago a technique was developed to form low energy (typically eV), near-mono-energetic, beams of positrons in vacuum using the interactions of β^+-particles with solids. In essence, β^+s implanted into a solid will slow rapidly to reach very low (thermal, or nearly so) energies, whereupon they will diffuse in the medium, perhaps become trapped at a defect if such exists, before annihilating in the bulk *or* reaching a surface of the solid. It is the latter which may result in a low energy positron in vacuum since, as detailed by Schultz and Lynn[45], many materials possess a negative work function for positrons, such that once at a surface, they can be spontaneously liberated into vacuum with a kinetic energy in the eV-range. An accessible introduction to positron beam production and technology was given by Beling and Charlton[46] and also see the volume edited by Coleman[47] and Charlton and Humberston[48]:

The primary β^+-particles are derived from a radioactive source, and the most common isotope for this purpose is ^{22}Na, which is commercially available in activities of around 1.8 GBq (~50 mCi) and has a conveniently long half-life of 2.6 years. The process of low energy positron beam formation is normally referred to as moderation, since it involves energy-loss of the β^+s in the solid moderator. The most efficient positron moderator turns out to be solidified neon[49,50] and plating a ~μm thick neon film onto a ^{22}Na source capsule and holder can (depending upon the source activity) result in positron beams with intensities close to 10^7 s^{-1}, typically with kinetic energies, selected by biasing the source/holder, in the 1 – 100 eV range.

Positrons have been accumulated for antihydrogen formation by several experiments using the buffer gas technique pioneered by Surko and coworkers[51,52] and see also the summaries given by ATHENA and ALPHA[33,34]. A schematic illustration of the ALPHA positron accumulator is given in Figure 3, which shows a three-stage electrode arrangement immersed in a uniform magnetic field, which is directed along the axis of the instrument. Once trapped in the apparatus, the positrons are radially confined by the magnetic field and axially held by voltages applied to the electrode stack, as shown in the lower panel. This device is an example of an elongated Penning, so-called Penning–Malmberg, trap.

Since the positrons issue at random from the radioactive source/moderator combination, they cannot be dynamically captured using voltage-switching techniques in the manner described above to collect the $\bar{p}$s. Instead, the positrons can be held by promoting kinetic energy loss in the trap *via* collisions with deliberately introduced N_2 gas. This is done by admitting the gas into the first stage of the trap at a pressure of

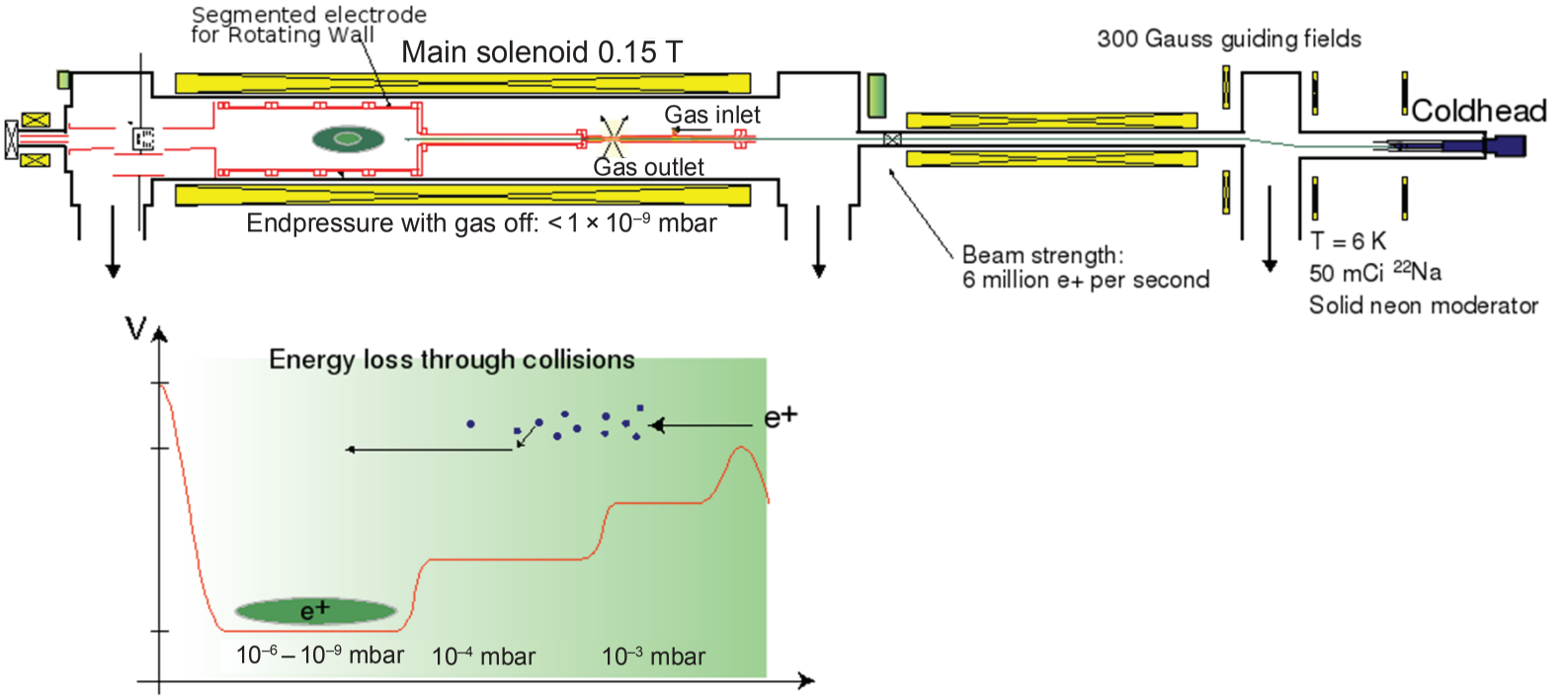

Figure 3 *Schematic illustration of the ALPHA buffer gas-based positron accumulator. The positron beam enters the three-stage electrode structure from the right over a small potential barrier. A positron excitation collision [reaction (5)] results in capture in the first stage, and subsequent collisions result in accumulation in the third stage, where the N_2 gas pressure is around 10^{-6} mbar. One of the third-stage electrodes is segmented to allow the application of a rotating electric field (see text). The solenoidal field is typically between 0.1 and 0.15 T and positrons can be ejected to the left for diagnosis using a phosphor screen/CCD camera system. The gas pressure gradient is maintained by cryogenic pumps at either end of the system, and when the N_2 gas flow into the apparatus is turned off the pressure in the final stage drops to 10^{-8}–10^{-9} mbar, whereupon transfer to the main ALPHA antihydrogen system (see Section 3) can be effected.*

around 10^{-3} mbar: differential pumping of the further two stages (of progressively wider electrode structures, as shown in Figure 3) provides a natural pressure gradient along the trap axis resulting in a three-order-of-magnitude drop in the third and final stage.

Positrons are captured after undergoing a collision involving energy loss of around 9 eV *via* electronic excitation of the N_2 gas as

$$e^+ + N_2 \rightarrow e^+ + N_2^*, \tag{5}$$

a reaction which competes effectively near threshold[53] with the positron loss channel of positronium formation,

$$e^+ + N_2 \rightarrow Ps + N_2^+. \tag{6}$$

Once captured, the positrons undergo further collisions according to reaction (5) in the second and third stages, and after a few μs reside in the latter[51] where they have lifetimes of the order of 100 s. Figure 4 shows typical positron accumulation curves, indicating that in excess of 10^8 positrons can be gathered within times of the order of $2-3$ minutes. After $10-15$ s of accumulation the positron cloud is sufficiently dense that they form a so-called single component plasma (see ref. 54 for a review of such objects) which can, as described later in this section, be further manipulated to facilitate antihydrogen formation. In any case, once the required number of positrons have been accumulated they can be efficiently transferred to the main part of the antihydrogen apparatus for interaction with the trapped antiprotons[55,56]. There the magnetic field is of the order of 1 T, so the positrons self-cool *via* the emission of synchrotron radiation to temperatures which can approach the ambient of the Penning traps, which are typically held in a cryogenic environment.

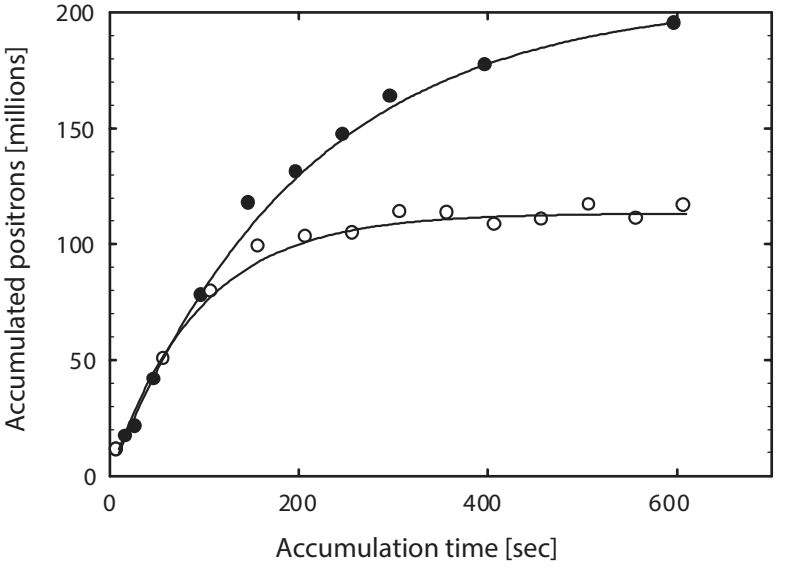

Figure 4 *Two examples of positron accumulation in the final stage of a buffer gas trap. The positron lifetime in the trap is around 100 s and is limited by annihilation on the N_2 gas and collision-induced cross magnetic field transport.*

Once captured and cooled the positron and antiproton clouds must be further manipulated before they are mixed, including the use of tailored electric fields applied to the confining electrode traps to reduce their radial extent. It is worthwhile here pausing to consider the nature of the positron and electron (used to cool the antiprotons, as described earlier) clouds in the Penning trap. The electron/positron numbers, densities (n_e) and temperatures (T_e) typical in antihydrogen experiments mean that these clouds are actually classified as being in the plasma state. This occurs when the Debye screening length, λ_D, given by

$$\lambda_D = \sqrt{\varepsilon_0 k_B T_e / n_e e^2} \tag{7}$$

with ε_0, k_B and e the permittivity of free space, Boltzmann's constant and the unit charge, respectively, is much smaller than any of the dimensions of the trapped ensemble. With the radial dimension being the smallest, and of order 1 mm, and with λ_D typically around $10-100$ μm, the trapped clouds are in the plasma regime, such that the trap voltages are effectively screened from the particles inside the cloud over penetration distances on the scale of λ_D. Thus, the relevant electric field is not that derived from the voltages applied to the trap electrodes, but the self-field of the plasma. This field is radial (r) in nature and it combines with the axial magnetic field in the trap to give so-called $\mathbf{E} \times \mathbf{B}$ effects which result in the plasma exhibiting a collective magnetron drift-like rotation about the magnetic field with an angular frequency, ω_D given by

$$\omega_D = E/rB = n_e e/2\varepsilon_0 B \tag{8}$$

with E the magnitude of the plasma self electric field. This translates into a tangential speed, v_T, for the particles in the plasma, which is proportional to their radial position, r as $v_T = \omega_D r$. It is notable that equation (8) has no dependence upon the mass of the particle, such that a more massive particle, such as an antiproton, which finds itself embedded in a rotating positron or electron plasma, will undergo similar motion, also with a characteristic angular frequency of ω_D. This will impart a kinetic energy to any antihydrogen formed from the antiprotons, which may preclude their capture in the neutral atom trap. We can quickly gauge the size of this problem, by estimating the radial position which will correspond to an effective kinetic energy of only 1 degree Kelvin. (Hopefully the reason for this choice will become clear in Section 3.) The relationship between the radial position of antihydrogen formation and the kinetic energy (in terms of temperature) imparted to it by virtue of the plasma rotation can be found by equating $m_{\bar{\mathrm{H}}} v_T^2/2$ to $k_B T_{\bar{\mathrm{H}}}$.

Thus,

$$r_{\bar{\mathrm{H}}} = \sqrt{(2k_B T_{\bar{\mathrm{H}}} / m_{\bar{\mathrm{H}}})}/\omega_D \tag{9}$$

which, using equation (8) and inserting the aforementioned $T_{\bar{\mathrm{H}}} = 1$ K and a typical value for the positron plasma density of $n_e = 10^{13}$ m^{-3} and magnetic field of 1 T, we find that $r_{\bar{\mathrm{H}}}$ must be below 1.5 mm to keep the antihydrogen temperature down. This observation, and the need to increase antihydrogen production efficiency by ensuring good overlap between the positron and antiproton clouds, has prompted the development of techniques to manipulate their radial extent. In particular the use of rotating electric fields, so-called rotating walls, as drive voltages phase-shifted with respect to one another and applied to a segmented Penning trap electrode, can be used to tailor the plasmas before mixing.

The rotating wall works by using the electric field to drive the plasma rotation in the direction of the natural $\mathbf{E} \times \mathbf{B}$ drift. This effectively applies a positive torque to the plasma, which spins it up: and since angular momentum is conserved, the plasma shrinks. Of course the driving fields heat the plasmas, and this energy needs to be removed, otherwise it would add an extra thermal component to the antihydrogen kinetic energy on formation. Fortunately, in the strong magnetic fields used to confine the plasmas, the positrons and electrons self-cool, as mentioned above, by the emission of synchrotron radiation on a timescale of a second or less.

The rotating wall technique was developed to modify the properties of electron plasmas (see for example refs 57–59), but has also found a number of applications with positron plasmas and clouds[55,60–63]. A particularly useful application of this technique was discovered by ALPHA who found that if rotating-wall compression of an electron plasma with embedded antiprotons was done gently enough, then the latter shrank alongside the lighter particles[64].

This sympathetic compression has the added benefit of providing a source of cooling (the radiating electrons) for the antiprotons. Figure 5 shows examples of how the antiproton and electron ensemble radii track one another during the application of the rotating wall. Once this manipulation has been completed, the electrons can be ejected to leave a sub-mm cool antiproton cloud ready for further manipulation and/or antihydrogen formation.

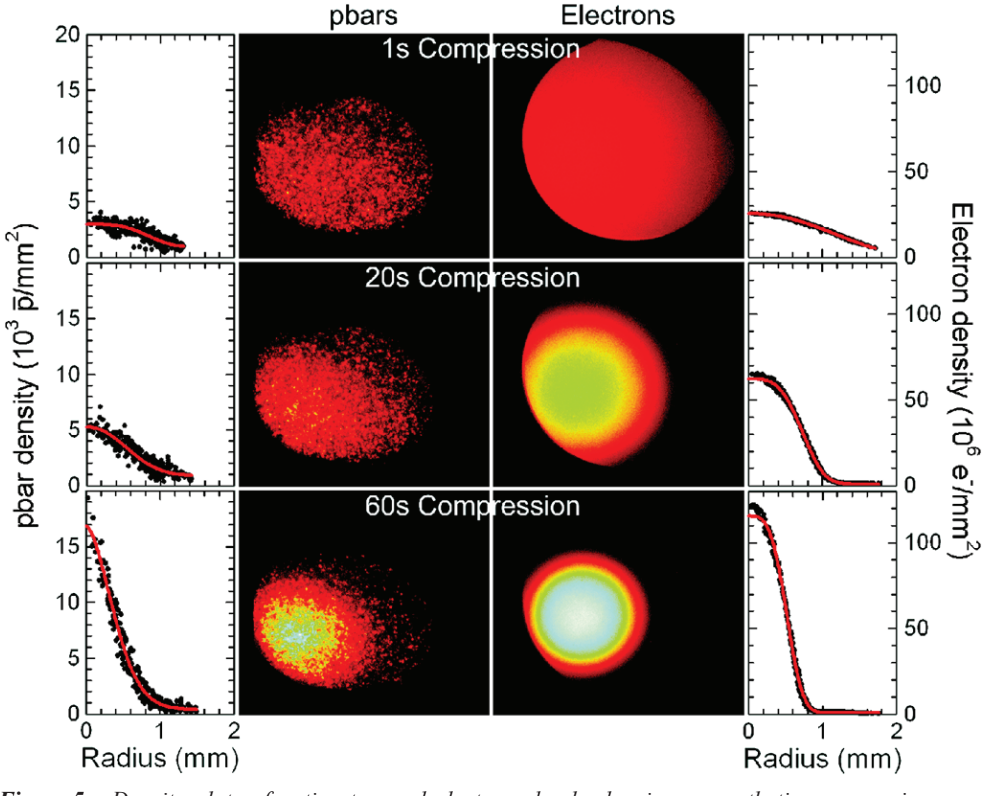

Figure 5 *Density plots of antiproton and electron clouds showing sympathetic compression, over many seconds, of the former by the latter. The red lines are Gaussian-type fits to the radial profiles; see ref 64 for more information.*

The properties of the antiparticle plasmas and clouds that are important for the formation of antihydrogen are the total numbers of each antiparticle, their densities, radial extents and their ensemble temperatures. Techniques to track some of these, based, for instance, upon monitoring the frequency-dependent collective motions of the plasmas and utilising sophisticated descriptions of the electrostatic plasma behaviour, have been developed by the various antihydrogen collaborations. The technical details are beyond the scope of this article, but we note that particle numbers and plasma geometries can be obtained using *in-situ* diagnostics with sufficient accuracy for the current level of requirements for antihydrogen production.

However, of greater relevance for antihydrogen trapping are the antiproton and positron ensemble temperatures and, in particular, the latter, as this is one of the factors governing the antihydrogen kinetic energy on production, and hence the likelihood that the antiatom can be held in a neutral atom magnetic minimum trap less than 1 K deep. ALPHA has developed a temperature diagnostic based upon the technique of Malmberg and co-workers[65,66]. Here the trapped cloud or plasma is released by gradually lowering one side of the electrostatic confining well and the integrated yield of liberated particles *versus* the well depth is measured. It can be shown that the initial particles released originate from the exponential tail of the Maxwell–Boltzmann energy distribution of the plasma, provided the cloud is in thermal equilibrium. Fitting the particle yield can thus be used to determine the cloud/plasma temperature (see below for examples). Small corrections are often applied to the directly extracted values to account for effects such as the time-dependence of the vacuum electrical potentials and the self-field of the plasma, as detailed by Andresen *et al.*[67].

The ALPHA temperature diagnostic has been applied to derive plasma and/or cloud temperatures for trapped samples of electrons, positrons and antiprotons, and was put to good use in the process of evaporative cooling[67] to facilitate the production of clouds of cryogenic antiparticles for antihydrogen creation for trapping. In these experiments, antiparticles were released as one side of an electrostatic well, in this case for antiprotons, was reduced, from an initial value of 1,500 mV down to a lowest value of just (10 ± 4) mV. The voltage reduction was staged, and each stage resulted in the hotter antiprotons escaping. Those remaining were held for a sufficient time to reach thermal equilibrium *via* collisions, but now at a lower temperature consistent with the reduced trapping voltage. Repeating this process several times resulted in ever lower antiproton temperatures, though at the expense of depletion of the trapped sample. Figure 6 shows the integrated antiproton loss and the exponential fits used to derive the cloud temperature. From here it is clear that antiproton temperatures around 10 K have been achieved with around 6% of the initial number remaining. Similar trap manipulations have also been used to cool positron clouds to around 40 K, and these were used to prepare the cold plasmas for antiproton insertion to occur, as will be described in Section 3.

ATRAP has recently devised an efficient method to lower the temperature of antiproton clouds based upon the principle of adiabatic cooling[68]. This method has the advantage of being loss-free and has produced a plasma of over 3×10^6 antiprotons at temperatures as low as (3.5 ± 0.7) K. In this technique, a combined antiproton-electron cloud was held together in a quasi-harmonic Penning trap but, instead of the usual situation for sympathetic cooling using electrons (see above) in which the latter are much more numerous than the antiprotons, here the antiprotons dominate. Nevertheless,

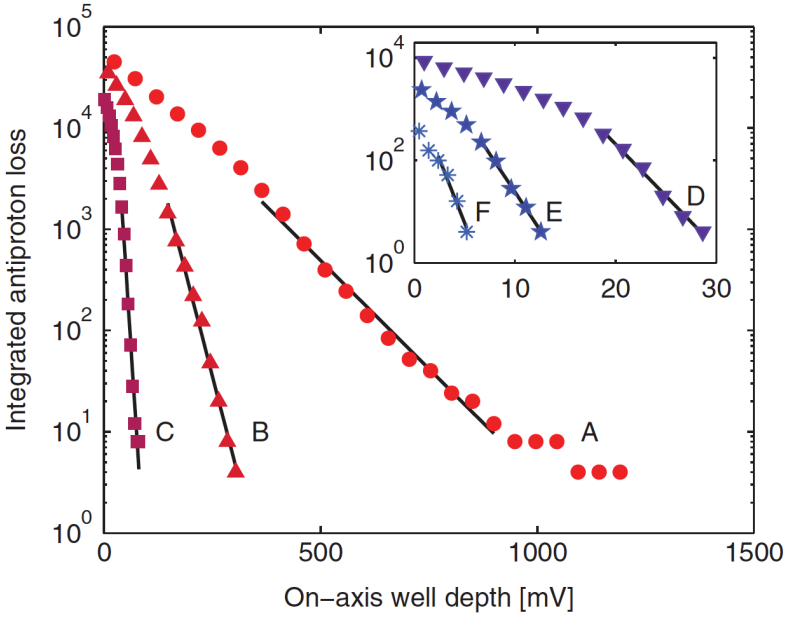

Figure 6 *The integrated number of antiprotons lost from various electrostatic wells plotted* versus *the dynamic well depth. The curves are labelled according to the antiproton temperature derived from the exponential fits, which are shown as the solid lines. The temperatures (in kelvin) are: A, 1040; B, 325; C, 57; D, 23; E, 19 and F, 9. For the shallowest well 6±1% of the initial sample of 45,000 antiprotons remain in the cooled ensemble.*

the co-trapped electrons still cool the antiprotons, though on a longer timescale, as they themselves self-cool by the emission of synchrotron radiation; this is necessary to reduce the antiproton temperature before adiabatic cooling, but after other preparatory manipulations of the plasma. Furthermore, the electrons are sufficiently few in number that the trap dynamics are dominated by the antiproton plasma, which is collected by stacking AD pulses[69].

The cooling works by holding the antiprotons in a deep well which is slowly lowered and expanded in length (along z), and hence volume, and in the process lowering the restoring force, F_r, and internal energy, U_p, of a plasma initially at a temperature T_i. The key physics has been nicely summarised by Gabrielse *et al.*[68]: a measure of both $F_r = mw_z^2 z$ and $U_p = mw_z^2 z^2/2$ (with m the antiproton mass) is the axial oscillation frequency, $f_z = \omega_z/2\pi$, which is reduced from an initial value f_{zi} to a final value f_{zf} in the adiabatic trap expansion, thereby lowering the temperature of the particles to T_f. The details of the relationship of the ratios (T_f/T_i) and (f_{zf}/f_{zi}) are somewhat involved, and depend upon the particular situation, and whether the plasma can be considered as an ideal gas, and details can be found in Gabrielse *et al.*[68]. Nonetheless, the cooling has been found to follow a power-law form, and the expected feature of negligible (or no) particle loss has been demonstrated.

3. Creating, trapping and beaming antihydrogen

The basic physical mechanisms used to create antihydrogen have been described in Section 2. The main method used to date involves the direct mixing of cold plasmas/

clouds of positrons and antiprotons to form the $\overline{H}$; it is thought typically *via* reaction (2). This method was pioneered by ATHENA,[70] and ATRAP,[23] although the details of the mixing procedures differed.

In the ATHENA case, around 10^4 $\bar{p}$s with a kinetic energy in the range 15 – 30 eV were launched into a positron plasma of typical density of 3×10^{14} m^{-3}. The positron plasmas were prolate spheroids with typical lengths of around 15 mm and diameter of 3 mm; the latter was less than that of the antiprotons, such that only a fraction of them overlapped with the positrons on mixing. Note: the $\bar{p}$ compression techniques described in Section 2.2 had not been developed when ATHENA performed these experiments. ATHENA found that the $\bar{p}$ kinetic energy lowered quickly on interaction with the positrons (whose temperature was, unfortunately, not measured directly), and that antihydrogen began to form after a few 10s of ms,[21] at rates in excess of 400 s^{-1} [71]. However, analysis of the axial (*i.e.*, the *z*-axis) distribution of the antihydrogen annihilation positions[72] found that it was much broader than expected from isotropic formation and emission from a positron plasma, even with extremely high assumed temperatures of the latter. The basic conclusion was that the antihydrogen was formed before the $\bar{p}$s had cooled within the plasma, such that a fraction of their injection energy remained upon formation. Although this was no barrier to antihydrogen production, this placed a formidable obstacle before any trapping effort, such that new modes of positron-antiproton mixing had to be devised.

For the ATHENA experiment the antihydrogen was detected *via* its annihilation. Once formed, it was no longer confined by the electromagnetic charged particle traps and much of it migrated directly to the walls of these traps, whereupon it annihilated on contact. This resulted in simultaneous (in space and time) characteristic antiproton and positron annihilation events: the former involved the release of energetic charged pions, whilst the latter produced a pair of back-to-back 511 keV gamma rays. In the first ATHENA experiment[70] both of these events were registered using a purpose-built imaging detector (see, for example, ref 33); a reconstructed image of an antihydrogen annihilation is shown in Figure 7.

The initial discovery events such as those shown in Figure 7 came, however, at a cost in detection efficiency, since numerous constraints placed restrictions on the size and number of scintillators that could be accommodated to record the 511 keV gamma rays. As a result, the full antihydrogen annihilation reconstruction efficiency was only 0.25%. However, it was quickly established that there was very little background on the antiproton annihilation signal, particularly if the position of the so-called vertex was located, as shown in Figure 7. With the silicon detectors having a high efficiency for detection of the energetic pions, using the $\bar{p}$-only identification as a proxy for antihydrogen allowed much more rapid experimental progress to be made. ALPHA also uses the $\bar{p}$ annihilation signal to detect antihydrogen[34] using a similar silicon strip detector, but now with three layers rather than two, which allows better event reconstruction since the curved trajectories of the charged pions in the strong magnetic fields used in the Penning and neutral atom traps can be monitored.

Most antihydrogen experiments are now performed using a method to mix positrons and antiprotons based upon exciting the axial motion of the trapped antiprotons. As mentioned in Section 2.1 a charged particle, or ion, held in a Penning trap oscillates along the axis of the trap with a characteristic (so-called bounce, or axial) frequency, f_z, that is governed by the charge-to-mass ratio of the species and the physical size

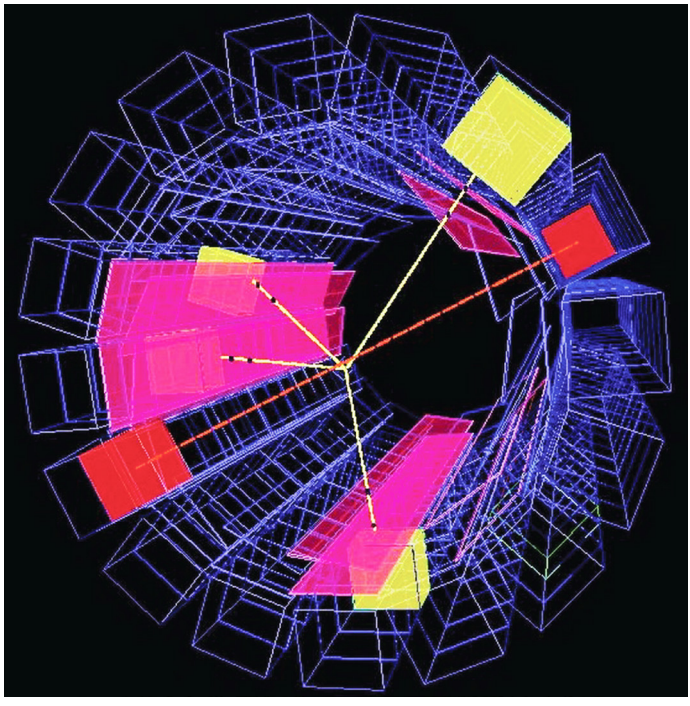

Figure 7 *Antihydrogen annihilation in ATHENA. Shown in yellow are the reconstructed tracks of the pions, as registered by a double layer of silicon strip detectors. In red are the pair of gamma rays emitted in electron-positron annihilation as monitored using a bank of 192 miniature scintillation detection devices.*

and electrical depth of the trap[35]. If a drive voltage is applied to a trap electrode at the antiproton bounce frequency their amplitude of oscillation will increase. As a consequence, however, the antiproton trajectories will encompass anharmonic regions of the trap, where f_z is lower, such that they come out of lock with the drive. The conclusion is that a single drive frequency will not result in the antiprotons being able to leave the trap to mix with positrons held in a nearby well.

ALPHA has overcome this using a technique based upon the phenomenon known as autoresonance[73,74] in which a chirped frequency excitation is used. Here the excitation frequency is started at a value above f_z, and then lowered (chirped) at a constant rate. As the frequency passes through f_z the antiproton locks to the drive and remains so as the excitation becomes larger, and the frequency is reduced further, until the antiproton gains just enough energy to depart from its trap, whereupon it is able to enter the region containing the positrons. This advance enabled some antihydrogen to be created with low enough kinetic energies to allow capture in a magnetic minimum trap, as will be described later in this section.

It is also possible to heat trapped particles by applying broad-band radio frequency (r.f.) excitation, as demonstrated by ATHENA in their studies involving (i) antihydrogen formation at different positron cloud temperatures[75] and (ii) the temporal modulation of antihydrogen formation[43]. Such a technique was also used by ATRAP to drive antiprotons into a positron cloud for antihydrogen formation. In that case, the r.f. was applied alternately between a pair of electrodes to drive the $\bar{p}$s across an arrangement of

Penning traps. Once the antiprotons were inside the positron cloud, they cooled and antihydrogen was formed during this period. Further discussion of this, and related techniques, is given elsewhere[24,76,77].

ATRAP also developed a method of detecting antihydrogen formation, but without using the annihilation signals. The technique exploited the fact that antihydrogen created *via* the three-body reaction [equation (2)] is very weakly bound and can be ionised by electric fields that can easily be accommodated into the Penning traps. The relevant fields have strengths of around a few 10^3 V m^{-1}, which corresponds to the Coulomb field between singly charged particles separated by around 1 μm or an atom bound by about a meV.

A schematic of the ATRAP electrode system, together with the on-axis (the axis of symmetry along the trap electrodes and parallel to the applied solenoidal field) electrical potentials, is given in Figure 8. For our purposes, the important electrical well is the one on the right of the positron–antiproton interaction region. By ensuring that no charged particles could reach this well, the only way in which it could be filled with antiprotons is if they had been transported there in an electrically neutral entity (*i.e.*, antihydrogen) and then field-ionised *in-situ* by the electric field. Essentially, ATRAP monitored the contents of this well (by periodically emptying it and counting the antiprotons) as a means of detecting antihydrogen; see Figure 8. Analysis of the electric field dependence of the signal from the well was used to deduce information regarding the antihydrogen binding energies, as has been summarised elsewhere[76].

A long-term goal of antihydrogen physics is to perform spectroscopy on the antiatoms to compare their properties with those of hydrogen. As such, it has been anticipated for some time that, for this purpose, antihydrogen would be held in a neutral atom trap. This would enable long interrogation times, which it is hoped would compensate for the much lower sample numbers of antiatoms (when compared to their matter counterparts). Also, it would ensure, if the antihydrogen atoms could be held for around a second or so, that they were all in their ground (1S) state, which is the preferred initial state for spectroscopy.

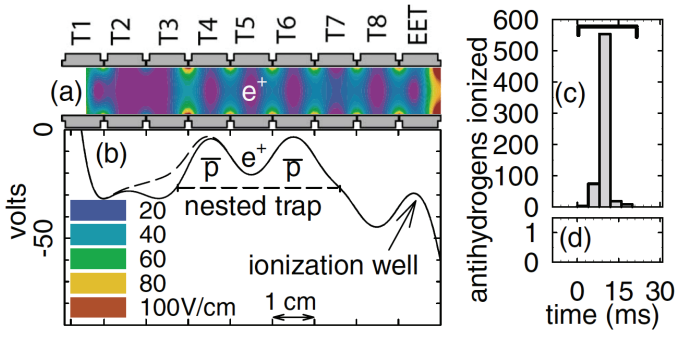

Figure 8 *(a) Schematic illustration of the ATRAP electrodes with colour-coded electric fields. (b) The electrical potential on the axis of the electrode stack, showing the respective positions of the positron and antiproton clouds and with the ionisation well to the right. (c) The background-free* $\bar{p}$ *annihilation signal obtained when the ionisation well was emptied. (d) No ionisation well signal is present when there are no positrons used in the experiments. Reproduced by permission from ref. 23* ©*American Institute of Physics.*

Recently two collaborations, ALPHA and ATRAP, have demonstrated that small quantities of antihydrogen atoms can be held in magnetic minimum traps for periods in excess of 1,000 s if desired[77–80]. The ALPHA set-up has already been shown in schematic in Figure 1, with the principle behind magnetic trapping described in Section 2.1. The level of detail presented there is sufficient for the present purposes, where the somewhat different coil configurations used by the two collaborations are also described.

ALPHA was the first to succeed in trapping antihydrogen. The experiments proceeded along the following lines. The positrons and antiprotons were collected, cooled and manipulated as described in Section 2.2 and then mixed for 1 s using the autoresonance technique described earlier in this section. Once the mixing cycle was complete the charged particles were swept from the trap by applying a sequence of electric fields, which would of course have no effect on the charge-neutral antiatoms. Thereafter, following a pre-set, though variable, antihydrogen hold time, the magnetic minimum trap was turned off to allow any trapped antihydrogen atoms to migrate to the wall of the trap and annihilate. Removing the large currents circulating in the superconducting coils used to provide the atom trapping fields was a technical challenge, but ALPHA succeeded in doing this with a $1/e$ time constant of just below 10 ms. This allowed the annihilation detectors to be interrogated for antihydrogen signals in a 30 ms time window after the initiation of shutdown, which helped to reject cosmic rays, which are a source of background counts in the ALPHA annihilation detector.

Figure 9 shows the reconstructions of both antihydrogen (actually the antiproton in the antiatom) annihilations, and an example of a cosmic ray event. It proved possible to discriminate efficiently against the latter (which were recorded at a d.c. rate of

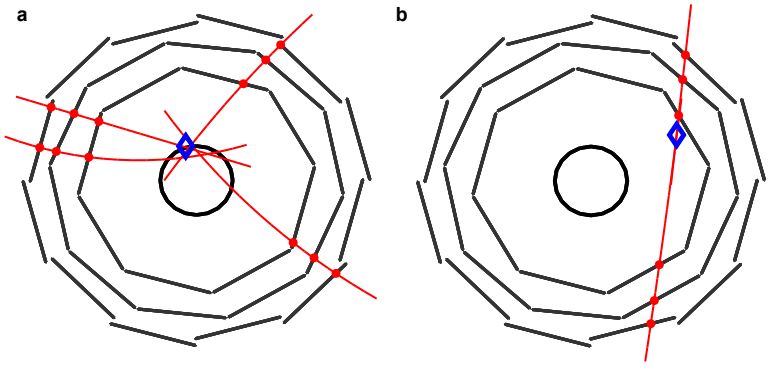

Figure 9 *ALPHA data illustrating reconstructions of (a) an antiproton annihilation as a result of antihydrogen formation and (b) a cosmic ray. The three layers of the ALPHA silicon detector are shown in section, with the black inner circle corresponding to the location of the charged particle trap electrodes (which also form the walls of the antihydrogen trap). The red dots denote the points of intersection of charged particles traversing the silicon modules of the detector. In the antihydrogen case this allows the pion tracks to be reconstructed, and then back-projected to their common point of origin, the so-called antiproton annihilation vertex, and denoted by the blue diamond. Note that the event reconstruction algorithm can locate a false vertex due to a cosmic event, as shown in (b). Fortunately the dissimilar topology of the two events, and the fact that antihydrogen annihilations only occur at the trap wall, whereas the cosmic tracks appear to intersect throughout the volume of the instrument, allows rejection of a large fraction of the cosmics, with manageable loss of efficiency for antiproton vertex location.*

around 10 s^{-1}), which, coupled with the 30 ms time window, allowed the signal from the very rare trapped antiatoms to be isolated. The original trapping report[78] detailed the detection of the release of just 38 trapped antihydrogen atoms, which required the development of stringent procedures to discriminate against antiprotons that may be trapped in the electromagnetic fields of the various traps[81].

Subsequently, ALPHA reported the detection of around 400 trapped antiatoms, with various hold times up to 2,000 s[79]. Figure 10 shows the distribution of annihilation locations in z (*i.e.*, along the axis of the instrument – see Figure 1) and in time after the initiation of the magnet shutdown, for various hold times. The experimental distribution is very similar in form to the results of simulations also shown in Figure 10. The long hold times of the trapped antihydrogen guarantees that it reaches the ground state, as required for experimentation. This trapping has allowed the first investigations of the properties of antihydrogen to be undertaken, as will be described in Section 4, and bodes well for future advances in precision spectroscopy of the antiatom.

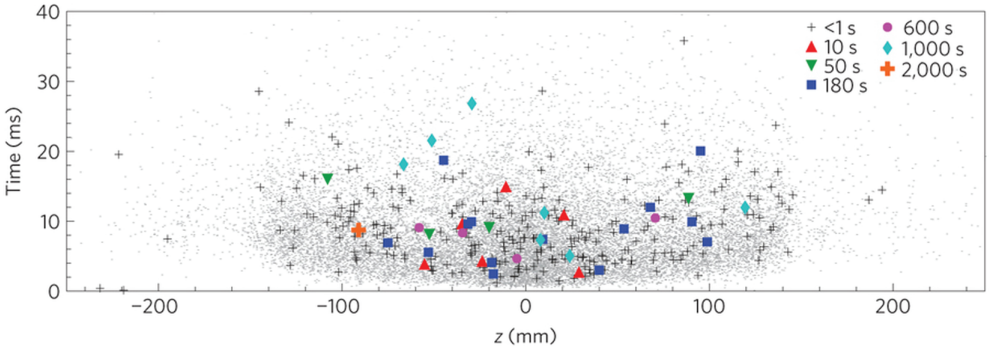

Figure 10 *Antihydrogen annihilation distributions in* z *and* t *as recorded during the atom trap shutdown in the ALPHA experiment*[79]*. The colour key shows the different hold times, which is the time after the end of positron–antiproton mixing to the initiation of the magnet shutdown. The numerous grey symbols are the result of trajectory simulations using the antihydrogen equations of motion in the changing magnetic field.*

The ASACUSA collaboration is also host to an antihydrogen effort that recently succeeded in producing the antiatom[82] and detecting it 2.7 m downstream from the place of formation[83]. This group is motivated to produce a beam of ground state antihydrogen atoms in order to perform (hyperfine) spectroscopy (see, for example, ref. 84) in a region free of the type of strong fields used to trap and manipulate the antiparticles and antiatoms. Such a methodology is akin to atomic and molecular beam techniques pioneered many years ago by Rabi and Ramsey and collaborators (see, for example, ref. 85). The positron–antiproton mixing was performed in a manner similar to that developed by ATHENA and ALPHA, though the magnetic field configuration used was quite different; a so-called cusp trap comprised of anti-Helmholtz magnetic coils and a multi-ring electrode charged particle trap[86]. A detailed analysis of the magnetic field produced in a cusp trap, and ground state antihydrogen trajectories, has shown that an antiatom beam emitted from the device, and along its axis, is preferentially spin-polarised[87], as is required for the proposed measurements on the antihydrogen hyperfine

states. To date, a total of 80 antihydrogen atoms have been located at distance from the cusp trap, and a field ionisation analysis of the distribution of states has established that a fraction of them occupy states with principal quantum number less than 29, though with low count rate at present. Nonetheless, this is a first step towards the study of the structure of antihydrogen using beam-based techniques.

Before concluding this section it is worth noting that a method of producing antihydrogen using positronium atoms has already been demonstrated, and that two other groups intend to use a positronium route in future. ATRAP have performed a proof-of-principle experiment[88,89] in which laser-excited Cs atoms were used in a charge exchange reaction with a cloud of positrons to produce excited state positronium. A sample of these then went on to interact with trapped antiprotons to produce antihydrogen. A schematic of this is shown in Figure 11. Though only 14±4 antiatoms were identified in the initial experiment, the use of charge exchange reactions does produce a series of well-defined antihydrogen states, and the inherently lower recoil of the nascent antiatoms may promote more efficient trapping, though much work remains to probe these matters further.

The AEgIS collaboration has set a first goal of measuring the acceleration due to gravity, g, for antihydrogen to an accuracy of around 1%[17]. This is already a challenging proposition, and a schematic of the principle of the experiment, which relies upon applying the technique of neutral atom Moiré deflectometry[90] to antihydrogen, is shown in Figure 12. For this purpose, a well-defined beam of antihydrogen atoms must be produced and the basis is the production of antihydrogen using reaction (3), but with the positronium laser-excited to a Rydberg state[28]. The aim is to cool antiprotons, hopefully to a very low temperature of around 100 mK by a variety of techniques, such as those described in Section 2.2, though the development of a variant of sympathetic cooling using laser-cooled negative ions[91] may be needed to accomplish this. The low

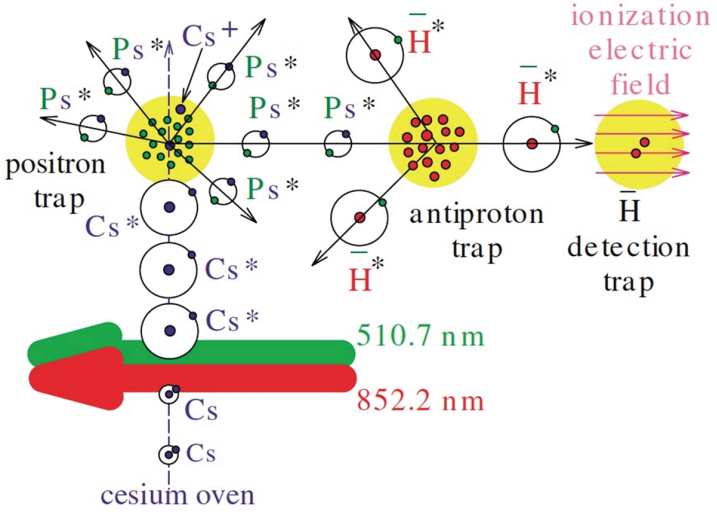

Figure 11 *Schematic illustration of the ATRAP double charge exchange route for antihydrogen formation. Cs atoms emanating from an oven were laser excited to high-lying atomic states. Interaction with the trapped positron clouds produced Rydberg Ps atoms, some of which then collided with the nearby antiprotons to form $\overline{H}$. Reproduced by permission from ref. 89 ©American Institute of Physics.*

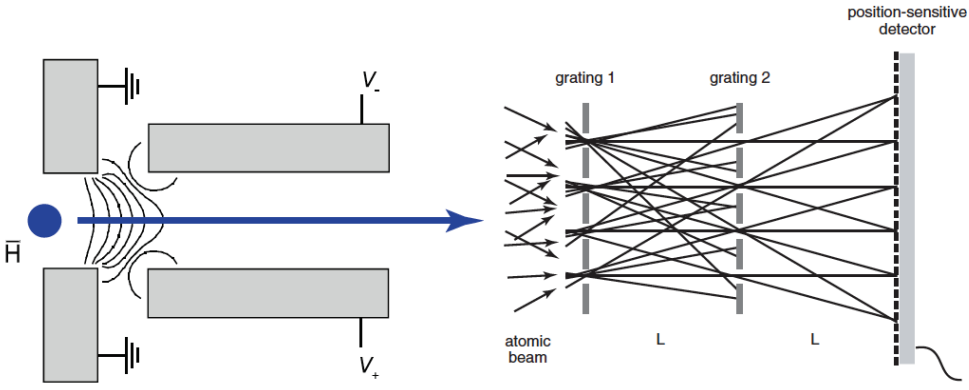

Figure 12 *Schematic illustration of the AEgIS experiment to measure* g *for antihydrogen. Reproduced by permission from ref. 17 ©IOP Publishing.*

antiproton temperature is required to ensure that the transverse antihydrogen speed, which will cause angular divergence of the antiatom beam, is kept as low as is feasible.

AEgIS will produce positronium atoms in a short burst by using the pulsed output of an ATHENA/ALPHA-style positron accumulator, which is currently in operation in the experiment[30] (along with an antiproton catching trap). The positronium will then be excited in two stages: from the $n_{Ps}=1$ to the $n_{Ps}=3$ state at 205 nm, followed by promotion into the range $n_{Ps}=20-25$ (1650–1700 nm)[92]. The beam will then be formed using the technique of Stark acceleration (see, for example, ref. 93) of the Rydberg antihydrogen and it is intended to have an horizontal speed of around 500 ms^{-1} (and a divergence of the order of 5°) which over a 1 m flight path results in a deflection due to gravity of about 20 μm[94].

The deflectometer, as illustrated in Figure 12, is to be comprised of two horizontal (physical) gratings, each with a 40 μm pitch, a device which is similar to one used[90] to measure g for argon atoms to a precision of 10^{-4}. The small deflection of the antiatoms poses challenges for detection, as the position of the beam needs to be measured, preferably with a resolution much smaller than the gravitational sag. AEgIS intends to use a novel emulsion detection scheme, which can efficiently register the antiproton annihilation vertices with 1–2 μm resolution, and vacuum operation and cryogenic tests have recently had some success[95].

CERN's other major antihydrogen gravity experiment is GBAR (see, for example, Pérez and Sacquin[18]), which is currently in off-site preparation and will rely for its operation upon the increased low energy antiproton flux available at the up-coming ELENA facility (see Section 5). The aim of GBAR is to make ultra-precise measurements of g for antihydrogen (eventually to around a part in 10^3) using a scheme involving the creation of ultra-cold antihydrogen[96–98]. The principle is to form the antihydrogen positive ion, $\overline{H}^+$, *via* consecutive charge exchanges involving positronium. In the first, antiprotons form antihydrogen according to reaction (3), which is then followed by the antihydrogen capturing a positron to form $\overline{H}^+$ in a further interaction as described in Section 2.1.

There are major challenges in this endeavour, including the need to produce a dense positronium cloud (in the range $10^{11}-10^{12}$ cm^{-3}) in order to reach a useful flux of $\overline{H}^+$. Currently, this can only be accomplished if a purpose-built intense positron source is

available, and test experiments for this are underway at CEA-Saclay[97]. Once produced (in a beam-like configuration) the antihydrogen ions will be slowed and then captured in a succession of charged particle traps[98]. For instance, the ions will be created at an equivalent temperature of the order of 10^7 K, but need to be cooled by about 11 orders of magnitude for the experiment to be performed to the desired specification. It is planned to achieve this in two stages: both involve sympathetic cooling (see the discussion of similar cooling in Section 2.2) using laser-cooled beryllium ions. In the first stage a so-called Paul trap is to be used, and numerous Be^+ ions will be present. For the second phase, a single cold ion in a precision trap will be used in conjunction with Raman cooling (see ref. 99, chapter 9) to cool a single $\overline{H}^+$. Once the ion has been cooled (to about a few tens of μK), it is intended that the extra positron will be photo-detached by a short laser pulse. The remnant antihydrogen atom will then be free to fall in the Earth's gravitational field, and its trajectory will be timed over a distance of about 15 cm to determine g.

4. Experimentation with antihydrogen

The trapping of antihydrogen[77–80] is a major breakthrough in the field which will be the catalyst for many studies of the properties of antimatter, and comparisons with matter. To date, only ALPHA has reported measurements on antihydrogen[100–102]; accordingly, we will summarise these here.

The first was the report of the seminal observation of a quantum jump in the antiatom[100] involving transitions between different so-called hyperfine states. The expected levels of the ground state ($n = 1$) of antihydrogen when it is immersed in a magnetic field are shown in Figure 13; the so-called Breit–Rabi diagram. It can be

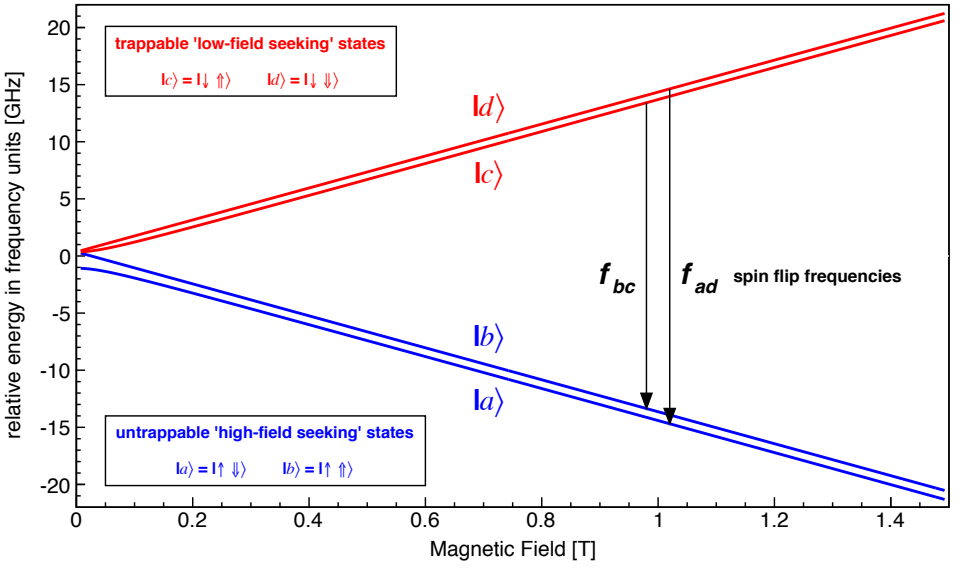

Figure 13 *Energy level diagram of the ground state of antihydrogen in an applied magnetic field. In the boxes the positron spins are labelled by the thin arrows, whilst those for the antiproton are thicker. See text for further discussion.*

seen from here that there are two hyperfine states, the singlet (total spin-zero) and triplet (spin-one), and that the energy degeneracy of the latter is lifted in the magnetic field. Thus, four states present themselves, labelled by convention $|a\rangle$–$|d\rangle$ and it is notable that the energies of $|c\rangle$ and $|d\rangle$ rise with B, whilst those of $|a\rangle$ and $|b\rangle$ fall. Referring back to the discussion in Section 2.1 of trapping of neutrals in magnetic fields it is clear that the low-field seeking states, and thus those able to be trapped, are $|c\rangle$ and $|d\rangle$ and that if transitions can be induced between these and the high-field seekers $|a\rangle$ and $|b\rangle$, the antihydrogen will immediately leave the trap and annihilate on the walls, producing an event like the one illustrated in Figure 9a. The transitions essentially involve positron spin flips, and are the equivalent of the famous electron spin resonances, the basis of techniques widely employed in materials physics and chemistry.

The transition frequencies in the 1 T field present at the minimum (*i.e.*, at the centre) of the antihydrogen trap are in the region of 28 – 30 GHz and this radiation was beamed down the axis of the trap by lowering a suitable microwave horn and associated instrumentation into the line-of-sight of the trap once the antihydrogen was held. The microwaves were applied in 15 s bursts, scanned in 15 MHz ranges about the two transition frequencies in succession, and both on- and off-resonance measurements were made, and comparisons were also made to results from trapping experiments with no microwaves present. It was found that when the microwaves were on resonance that virtually no antihydrogen remained in the trap when it was emptied as described in Section 3, and there was a marked difference between these data and those for the off-resonance and no microwaves cases. Furthermore, a detailed analysis of the time-dependence of the annihilation events during the application of the on-resonance microwaves revealed, as shown in Figure 14, an excess of annihilations which occurred during the very first of the pairs of 15 s scans. This is further, and very clear, evidence that the $|d\rangle$–$|a\rangle$ and $|c\rangle$–$|b\rangle$ transitions have been excited, resulting in ejection of antihydrogen from the trap.

In Section 3 it was shown how the z-distribution of antihydrogen annihilations was used by ALPHA to diagnose that the antiatoms had been trapped. Their detector also registered the y-positions (*i.e.*, up-down with respect to the axis; see Figure 1) of the annihilations, and it was natural to use those data to search for any signature of the gravitational sag of the trapped antihydrogen[101]. To do this the y-position data were compared with simulations of the motion of the antihydrogen in the trap which included the force due to the magnetic field gradient [*i.e*, equation (4)] and that due to gravity. The resulting equation of motion can be written as

$$M\frac{d^2\boldsymbol{\rho}}{dt^2} = \nabla\left(\boldsymbol{\mu}_{\overline{\mathbf{H}}}\cdot\mathbf{B}\,(\boldsymbol{\rho},t)\right) - M_g g\hat{\mathbf{y}} \tag{10}$$

where M and M_g are the antihydrogen inertial and gravitational masses respectively (which should be equal according to the Weak Equivalence Principle when applied to antimatter) and $\boldsymbol{\rho}$ is the position of the antihydrogen centre of mass at a time t. The simulations were performed for varying values of $F = M_g/M$ to assess sensitivity and explore systematics. (Note: a quick calculation will confirm that for $F = 1$ the expected gravity sag is only of order 10s of microns in ALPHA's magnetic minimum trap.) The y-distribution is plotted against time after magnet shutdown [essentially the t in equation (10)] in Figure 15.

In order to make best use of all the available data (for just 434 antihydrogen atoms in total), and as is evident from Figure 15 the effects of gravity are accentuated at longer

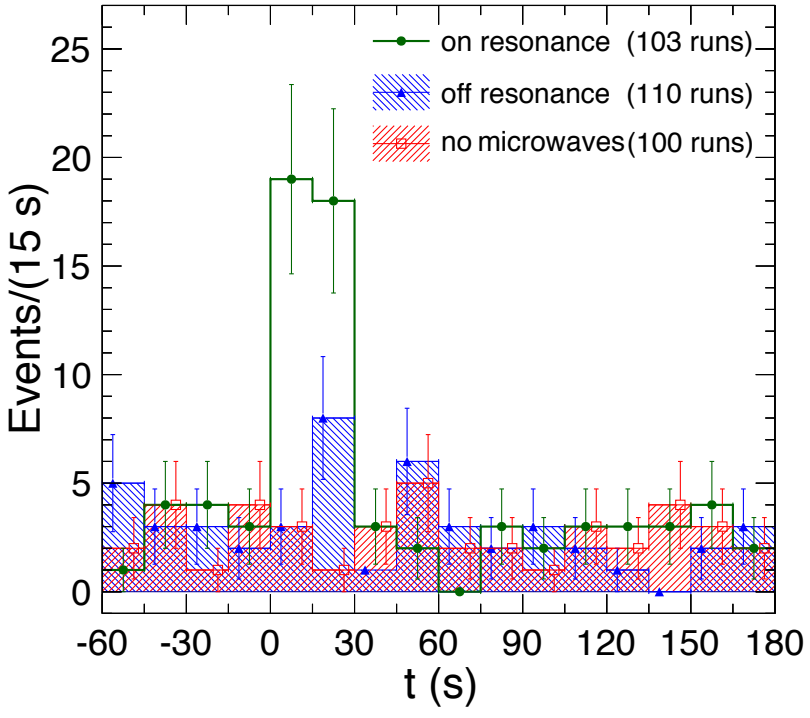

Figure 14 *Antihydrogen annihilations on the trap walls following ejection* via *the resonant excitation from the trapped to the untrapped quantum states. There is a clear excess of events in the first pair of 15 s microwave bursts.*

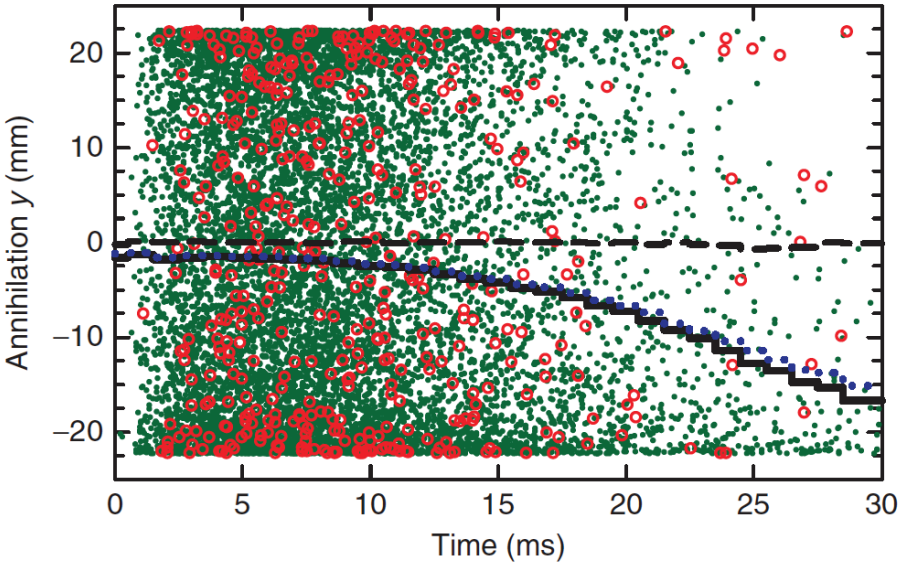

Figure 15 *The* y*-distribution of antihydrogen annihilations (red open dots) as recorded by ALPHA during the time after the neutral trap removal. The green dots are the results of the simulations using equation (10). The black lines are the average positions from simulation for values of* F = *1 (dashed line) and 100. The blue dotted line just visible near the* F = *100 results is with the effect of smearing included due the finite position resolution of the annihilation vertex detection.*

times as the slower antiatoms leave the decaying trap, ALPHA plotted their results in the form of a reverse cumulative average. This is denoted as $\langle y|t\rangle$ the average of the y annihilation positions that occur at a time t and after. These are shown in Figure 16, where the x-distributions, which will have no gravitational effect, are also shown for comparison.

From Figure 16 it is clear that the experiment has insufficient sensitivity to make statements concerning antimatter gravity near $|F|=1$, but that the data are clearly distinguishable from expectations (based upon the simulations) if $|F|=150$ is assumed.

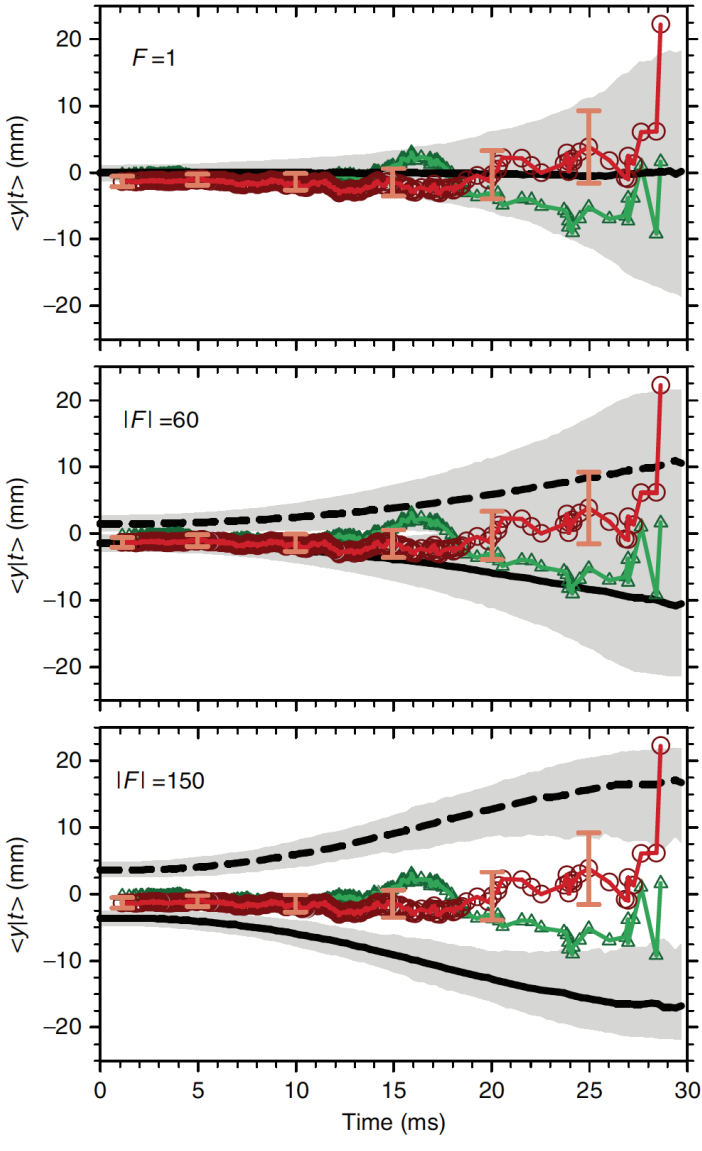

Figure 16 *Reverse cumulative averages* versus *time for 434 antihydrogen atoms: the red data are* $\langle y|t\rangle$*, with* $\langle x|t\rangle$ *shown in green. For comparison the results of simulations for* 9×10^5 *antiatoms for three absolute values of* F *are also shown with the black solid line denoting* $\langle y|t\rangle$*; the dotted line is its mirror about zero and corresponds to the case of antigravity. The grey shaded areas correspond to 90% confidence regions.*

ALPHA[101] made detailed arguments based upon careful statistical and systematic analyses to reject values of F greater than 75 (statistics only) or 110 if systematics were included in a worst case scenario. They also discussed potential improvements to allow the technique to probe near the more interesting $F=\pm 1$ region.

ALPHA have also published an analysis of the z-distributions of their annihilation data in which the electric fields used to clear charged particles, and which were present during the antihydrogen trap shutdown, were used to set a limit on a putative electric charge of antihydrogen, denoted by Q (in units of the elementary charge, e).[102] That such fields offer sensitivity to Q, can be seen straightforwardly: if Q is non-zero, the on-axis potential energy of the antihydrogen, $U(z)$, will be shifted away from the trap centre ($z=0$). For the case of charged antihydrogen $U(z)$ is given by

$$U(z)=\mu_{\bar{\mathrm{H}}}B(z)-QeEz/k_B. \tag{11}$$

Here, as introduced in Section 2.1 $B(z)=B(0)-\beta z^2$, with $B(0)$ the maximum field and β the coefficient describing the field variation due to ALPHA's mirror coils (see Figure 1). Note also that here we take $\mu_{\bar{\mathrm{H}}}=\mu_B=0.67\ \mathrm{KT}^{-1}$. By considering ejection/bias fields, E_L and E_R to the left and right (along z) respectively, an expression for Q can be found as

$$Q=\frac{4\mu_{\bar{\mathrm{H}}}\beta k_B}{e(E_R-E_L)}\langle z\rangle_\Delta, \tag{12}$$

with $\langle z\rangle_\Delta=0.5(\langle z\rangle_R-\langle z\rangle_L)$ where the $\langle z\rangle$s are the average annihilation positions with the fields to the right and left. This simple relationship indicates the level of sensitivity to even the modest fields used in the trapping experiments. Writing $Q=s\langle z\rangle_\Delta$, (with s the sensitivity), equation (12) gives $s=-3.7\times10^{-9}$ with $\langle z\rangle_\Delta$ in mm. This simple estimate was improved by ALPHA by performing detailed simulations of the complicated antihydrogen trajectories in the combination of the electric fields and the decaying magnetic trap fields, using equation (10), but with the term due to gravity replaced by one resulting from the putative charge as $Qe(\mathbf{E}(\boldsymbol{\rho},t)+\dot{\boldsymbol{\rho}}\times\mathbf{B}(\boldsymbol{\rho},t))$. This yielded $s=-(3.31\pm0.04)\times10^{-9}\,\mathrm{mm}^{-1}$, a value within 10% of the analytic result. When combined with ALPHA's antihydrogen annihilation z-distribution analysis, a result was found for Q which was consistent with zero (as expected) at a level of $Q/e=(-1.3\pm1.8\pm0.4)\times10^{-8}$. The first uncertainty quoted arose from statistics – *i.e.*, the precision with which the mean annihilation locations could be determined. The second uncertainty was due to possible systematic effects which were investigated in some detail by ALPHA using the aforementioned simulations. This precision obtained for Q was used together with the known proton/antiproton and electron/positron charge comparisons to allow the latter to be improved by a factor of around two[102].

5. Conclusions and outlook

This article has, hopefully, provided an accessible introduction to the state-of-the-art in low energy antihydrogen physics. Since the first controlled production of the antiatom *via* the merging of positron and antiproton ensembles in 2002 we have witnessed its trapping and long-time confinement, and the first developments of an antihydrogen beam (Section 3). As described in Section 4 this progress has already allowed the first experiments to be performed on the antiatom, and much more can be expected.

The long term goal of both ALPHA and ATRAP has been, and remains, to perform precision spectroscopy on antihydrogen for comparisons with equivalent transitions in hydrogen. As summarised in Section 1, a prime candidate is the 1S–2S two-photon Doppler-free transition, a line whose centre is known in hydrogen to the staggering precision of around 4 parts in 10^{15} [2]. The prospect of making antihydrogen measurements to this precision, and maybe even beyond, has long fuelled the experimental drive in this area. The ground-state hyperfine transition(s) are also of great interest: indeed excitation of a pair of these (unresolved) formed the first observation of a resonant quantum transition in antihydrogen[100]. In hydrogen this, so-called maser, transition is known to about 6 parts in 10^{13} [3], and noteworthy here are the plans from ASASUSA to investigate this in a hydrogen beam-like arrangement as described in Section 3.

There are many challenging scientific and technical issues to be addressed in these quests, for instance: interfacing the demanding laser/optical systems required for such precise frequency measurements with the complex, cryogenic environment needed to store antihydrogen; the inevitably low numbers of the antiatom when compared to the atom, which will present difficulties, both statistical and systematic (and whether in a trap or a beam) and for trapping experiments, issues of magnetometry in the strong (varying) field of the neutral atom traps (Section 2.1). There are bound to be many more, but big hurdles have already been overcome in the antihydrogen endeavour, and so far there is no sign of a showstopper – in fact, just the opposite.

We can also look forward to various experimental attacks on what might be termed $\bar{g}$, the acceleration of antimatter due to gravity. (It is also interesting to compare efforts with antihydrogen to those involving other antimatter-containing species, such as positronium and muonium; see ref. 103.) We have summarised ALPHA's first effort to derive *F,* the ratio of the gravitational and inertial masses of antihydrogen (*i.e*, equivalent to $F = \bar{g}/g$)[101], and further discussion of possibilities for this technique have been given elsewhere[104]. Longer term prospects involving atom interferometry have also received attention recently[105].

The methodologies adopted by both the AEgIS and GBAR collaborations to measure g have been briefly summarised herein (see Section 3). AEgIS have made solid progress, and have some crucial elements already in place at the AD (see refs 94, 95 and references therein), though many challenges remain, not least producing cold enough antiprotons to achieve the desired antihydrogen beam properties. Progress of the GBAR collaboration was also discussed recently[97,98] and a broad-ranging development programme in positron, laser and trapping physics is already underway in this respect.

It is fitting to end this article with the note to GBAR, since the operation of that experiment will test positron and antiproton capabilities to the limit. Indeed, in respect of the latter GBAR requires the ELENA facility for its operation. ELENA is a new Extra Low ENergy Antiproton ring which will decelerate the antiprotons from the AD kinetic energy of 5.3 MeV down to around 100 keV, with little loss in intensity (see for example ref. 106) and which should be in operation in 2017–18. The lower ejection energy of the ring is significant, as it will facilitate major changes to machine operation and to antiproton availability. At 100 keV the capture efficiency into Penning-type traps using the simple foil method described in Section 2.2 will increase by a factor of around 100 over that at 5.3 MeV, which should lead to commensurate enhancements in antihydrogen yields. Hopefully, along with other gains in antiatom trapping efficiency, this will result in major increases in trapped antihydrogen. The lower energy will also

allow the beamlines connecting ELENA to the experiments to operate using electrostatic deflection, rather than the magnetic devices in current use at the AD. This will provide for more flexibility in the time-scheduling of antiproton delivery (rather than in shift-like blocks at present), eventually giving experimenters more access to the beam and perhaps even facilitating further expansion of the AD programme. All in all, there are bright times ahead for this fast-developing field and we can look forward to many new physics results with antihydrogen in the near future.

Acknowledgements

The authors are grateful to all their collaborators, past and present, in ALPHA, GBAR and ATHENA for their roles in creating the exciting field of antihydrogen physics. We are also thankful for generous UK financial support over many years from the EPSRC, The Royal Society and the Leverhulme Trust. We also wish to acknowledge the support of staff and students at Swansea University.

References

1. Dirac, P.A.M. (1931) *Proc. Roy. Soc. Lond. A*, **133**, 60.
2. Parthey, G. *et al*. (2011) *Phys. Rev. Lett.*, **107**, 203001.
3. Essen, L., Donaldson, P.W., Bangham, M.J. and Hope, E.G. (1971) *Nature*, **229**, 110.
4. Adriani, O. *et al*. (2009) *Nature*, **458**, 607.
5. Adriani, O. *et al*. (2013) *Phys. Rev. Lett.*, **111**, 081102.
6. Aguilar, M. *et al*. (2012) *Phys. Rev. Lett.*, **110**, 141102.
7. Accardo, L. *et al*. (2014) *Phys. Rev. Lett.*, **113**, 112101.
8. Lüders, G. (1957) *Ann. Phys. Rev. (NY)*, **2**, 1.
9. Lüders, G. (1957) *Kong. Danske Vidensk. Selsk. Mat-Fys Medd*, **28**, 1.
10. Holzscheiter, M.H., Charlton, M. and Nieto, M.M. (2004) *Phys. Rep.*, **402**, 1.
11. Nieto, M.M. and Goldman, T. (1991) *Phys. Rep.*, **205**, 221.
12. Nieto, M.M. and Goldman, T. (1992) *Phys. Rep.*, **216**, 343.
13. Adelberger, E.G., Heckel, B.R., Stubbs, C.W. and Su, Y. (1991) *Phys. Rev. Lett.*, **66**, 850.
14. Maury, S. (1997) *Hyperfine Interact.*, **109**, 43.
15. Eriksson, T. (2009) *Hyperfine Interact.*, **194**, 123.
16. Hayano, R., Hori, M., Horváth, D. and Widmann, E. (2007) *Rep. Prog. Phys.*, **70**, 1995.
17. Doser, M. *et al*. (2012) *Class. Quantum Grav.*, **29**, 184009.
18. Pérez, P. and Sacquin, Y. (2012) *Class. Quantum Grav.*, **29**, 184008.
19. Robicheaux, F. (2008) *J. Phys. B, At. Mol. Opt. Phys.*, **41**, 192001.
20. Jonsell, S., van der Werf, D.P., Charlton, M. and Robicheaux, F. (2009) *J. Phys. B, At. Mol. Opt. Phys.*, **42**, 215002.
21. Amoretti, M. *et al*. (2004) *Phys. Lett. B*, **590**, 133.
22. Andresen, G.B. *et al*. (2010) *Phys. Lett. B*, **685**, 141.
23. Gabrielse, G. *et al*. (2002) *Phys. Rev. Lett.*, **89**, 213401.
24. Gabrielse, G. *et al*. (2002) *Phys. Rev. Lett.*, **89**, 233401.
25. Humberston, J.W., Charlton, M., Jacobsen, F.M. and Deutch, B.I. (1987) *J. Phys. B, At. Mol. Phys.*, **20**, L25.
26. Charlton, M. (1990) *Phys. Lett. A*, **143**, 143.
27. Deutch, B.I., Charlton, M., Holzscheiter, M.H., Hvelplund, P., Jørgensen, L.V., Knudsen, H., Laricchia, G., Merrison, J.P. and Poulsen, M.R. (1993) *Hyperfine Interact.*, **76**, 153.
28. Cassidy, D.B., Hisakado, T.H., Tom, H.W.K. and Mills Jr., A.P. (2012) *Phys. Rev. Lett.*, **108**, 043401.
29. Cassidy, D.B., Merrison, J.P., Charlton, M., Mitroy, J. and Ryzhikh, G. (1999) *J. Phys. B, At. Mol. Opt. Phys.*, **32**, 1923.
30. Krasnický, D. *et al*. (2013) *AIP Conf. Proc.*, **1521**, 144.
31. Major, F.H., Gheorge, V.N. and Werth, G. (2005) *Charged particle traps, physics and techniques of charged particle field confinement*. Springer, Berlin.

32. Ghosh, P.K. (1995) *Ion traps*. Clarendon Press, Oxford.
33. Amoretti, M. *et al*. (2004) *Nucl. Instrum. Methods Phys. Res. A*, **518**, 679.
34. Amole, C. *et al*. (2014) *Nuc. Instrum. Methods Phys. Res. A*, **735**, 319.
35. Brown, L.S. and Gabrielse, G. (1988) *Rev. Mod. Phys.*, **58**, 233.
36. Gott, Y.V., Ioffe, M.S. and Tel'kovskii, V.G. (1962) *Nucl. Fusion*, Pt 3 (2 Suppl.), **1045**.
37. Pritchard, D.F. (1983) *Phys. Rev. Lett.*, **51**, 1336.
38. Gabrielse, G. *et al*. (2008) *Phys. Rev. Lett.*, **100**, 113001.
39. Fajans, J., Bertsche, W., Burke, K., Chapman, S.F. and van der Werf, D.P. (2005) *Phys. Rev. Lett.*, **95**, 155001.
40. Gabrielse, G., Fei, X., Helmerson, K., Rolston, S.L., Tjoekler, R., Trainor, T.R., Kalinowsky, H., Haas, J. and Kells, W. (1986) *Phys. Rev. Lett.*, **57**, 2504.
41. Bosser, J. *et al*. (1997) *CERN PS/HP Note-97-36*.
42. Andresen, G.B. *et al*. (2008) *J. Phys. B, At. Mol. Opt. Phys.*, **41**, 011001.
43. Fujiwara, M.C. *et al*. (2008) *Phys. Rev. Lett.*, **101**, 053401.
44. Bailey, D.L., Townsend, D.W., Valk, P.E. and Maisey, M.N. (eds), (2004) *Positron emission tomography basic sciences*. Springer, New York.
45. Schultz, P.J. and Lynn, K.G. (1988) *Rev. Mod. Phys.*, **60**, 701.
46. Beling, C.D. and Charlton, M. (1987) *Cont. Phys.*, **28**, 241.
47. Coleman, P.G. (ed.). (2000) *Positron beams and their applications*. World Scientific, New York.
48. Charlton, M. and Humberston, J.W., (2001) *Positron physics*. Cambridge University Press.
49. Mills Jr., A.P. and Gullikson, E.M. (1986) *Appl. Phys. Lett.*, **49**, 1121.
50. Khatri, R., Charlton, M., Lynn, K.G., Mills Jr., A.P. and Roellig, L.O. (1990) *Appl. Phys. Lett.*, **57**, 2374.
51. Murphy, T.J. and Surko, C.M. (1992) *Phys. Rev. A*, **46**, 5696.
52. Surko, C.M. and Greaves, R.G. (2004) *Phys. Plasmas*, **11**, 2333.
53. Marler, J.P. and Surko, C.M. (2005) *Phys. Rev. A*, **72**, 062713.
54. Dubin, D.H.E. and O'Neil, T.M. (1999) *Rev. Mod. Phys.*, **71**, 87.
55. Jørgensen, L.V. *et al*. (2005) *Phys. Rev. Lett.*, **95**, 025002.
56. Comeau, D. *et al*. (2012) *New J. Phys.*, **14**, 045006.
57. Danielson, J.R. and Surko, C.M. (2005) *Phys. Rev. Lett.*, **94**, 035001.
58. Anderegg, F., Hollmann, E.M. and Driscoll, C.F. (1998) *Phys. Rev. Lett.*, **81**, 4875.
59. Danielson, J.R., Surko, C.M. and O'Neil, T.M. (2007) *Phys. Rev. Lett.*, **99**, 135005.
60. Greaves, R.G. and Surko, C.M. (2001) *Phys. Plasmas*, **8**, 1879.
61. Funakoshi, R. *et al*. (2007) *Phys. Rev. A*, **76**, 012713.
62. Greaves, R.G. and Moxom, J. (2008) *Phys. Plasmas*, **15**, 072304.
63. Isaac, C.A., Baker, C.J., Mortensen, T., van der Werf, D.P. and Charlton, M. (2011) *Phys. Rev. Lett.*, **107**, 033201.
64. Andresen, G.B. *et al*. (2008) *Phys. Rev. Lett.*, **100**, 203001.
65. Eggleston, D.L., Driscoll, C.F., Beck, B.R., Hyatt, A.W. and Malmberg, J.H. (1992) *Phys. Fluids B*, **4**, 3432.
66. Beck, B.R., Fajans, J. and Malmberg, J.H. (1996) *Phys. Plasmas*, **3**, 1250.
67. Andresen, G.B. *et al*. (2010) *Phys. Rev. Lett.*, **105**, 013003.
68. Gabrielse, G. *et al*. (2011) *Phys. Rev. Lett.*, **106**, 073002.
69. Gabrielse, G. *et al*. (2002) *Phys. Lett. B*, **548**, 140.
70. Amoretti, M. *et al*. (2002) *Nature*, **419**, 456.
71. Amoretti, M. *et al*. (2004) *Phys. Lett. B*, **578**, 23.
72. Madsen, N. *et al*. (2005) *Phys. Rev. Lett.*, **94**, 033403.
73. Andresen, G.B. *et al*. (2011) *Phys. Rev. Lett.*, **106**, 025012.
74. Amole, C. *et al*. (2013) *Phys. Plasmas*, **20**, 043510.
75. Amoretti, M. *et al*. (2004) *Phys. Lett. B*, **583**, 59.
76. Gabrielse, G. (2005) *Adv. At. Mol. Opt. Phys.*, **50**, 155.
77. Gabrielse, G. *et al*. (2012) *Phys. Rev. Lett.*, **108**, 113002.
78. Andresen, G.B. *et al*. (2010) *Nature*, **468**, 673.
79. Andresen, G.B. *et al*. (2011) *Nature Phys.*, **7**, 558.
80. Andresen, G.B. *et al*. (2011) *Phys. Lett. B*, **695**, 95.
81. Amole, C. *et al*. (2012) *New. J. Phys.*, **14**, 015010.
82. Enomoto, Y. *et al*. (2010) *Phys. Rev. Lett.*, **105**, 243401.
83. Kuroda, N. *et al*. (2014) *Nature Commun.*, **5**, 3089.
84. Juhász, B. and Widmann, E. (2009) *Hyperfine Interact.*, **193**, 305.

85. Ramsey, N.F. (1956) *Molecular beams*. Oxford University Press.
86. Oshima, N., Kojima, T.M., Niigaki, M., Mohri, A., Komaki, K. and Yamazaki, Y. (2004) *Phys. Rev. Lett.*, **93**, 195001.
87. Mohri, A. and Yamazaki, Y. (2003) *Europhys. Lett.*, **63**, 207.
88. Hessels, E.A., Homan, D.M. and Cavagnero, M.J. (1998) *Phys. Rev. A*, **57**, 1668.
89. Storry, C.H. *et al*. (2004) *Phys. Rev. Lett.*, **93**, 263401.
90. Oberthaler, M., Bernet, S., Rasel, M., Schmeidmeyer, J. and Zeilinger, A. (1996) *Phys. Rev. A*, **54**, 3165.
91. Kellerbauer, A. and Walz, J. (2006) *New J. Phys.*, **8**, 45.
92. Castelli, F., Boscolo, I., Cialdi, S., Giammarchi, M.G. and Comparat, D. (2008) *Phys. Rev. A*, **78**, 052512.
93. Hogan, S.D. and Merkt, F. (2008) *Phys. Rev. Lett.*, **100**, 043001.
94. Krasnický, D. *et al*. (2014) *Int. J. Mod. Phys., Conf. Series*, **30**, 1460262.
95. Ariga, T. *et al*. (2014) *Int. J. Mod. Phys., Conf. Series*, **30**, 1460268.
96. Walz, J. and Hänsch, T.W. (2004) *Gen. Rel. Grav.*, **36**, 561.
97. van der Werf, D.P. (2014) *Int. J. Mod. Phys., Conf. Series*, **30**, 1460263.
98. Hilico, L., Karr, J.-P., Douillet, A., Delicato, P., Wolf, S. and Kaler, F.S. (2014) *Int. J. Mod. Phys., Conf. Series*, **30**, 1460269.
99. Foot, C.J. (2005) *Atomic physics*. Oxford University Press.
100. Amole, C. *et al*. (2012) *Nature*, **483**, 439.
101. Amole, C. *et al*. (2013) *Nature Commun.,* **4**, 1875.
102. Amole, C. *et al*. (2014) *Nature Commun.*, **5**, 3955.
103. *International Journal of Modern Physics Conference Series, Proceedings of the 2nd International Workshop on Antimatter and Gravity (WAG 2013)* (2014). World Scientific, New York.
104. Zhmoginov, A.I., Charman, A.E., Shalloo, R., Fajans, J. and Wurtele, J.S. (2013) *Class. Quant. Grav.*, **30**, 205014.
105. Hamilton, P., Zhmoginov, A., Robicheaux, F., Fajans, J., Wurtele, J.S. and Mueller, H. (2014) *Phys. Rev. Lett.*, **112**, 121102.
106. Bartmann, W. *et al*. (2014) *Int. J. Mod. Phys., Conference Series*, **30**, 1460261.